Morphing simulations reveal architecture effects on polymer miscibility

Shreya Shetty,[†] Milena M. Adams,[†,‡] Enrique D. Gomez,[†,‡,¶] and Scott T. Milner[*,†,‡]

†*Department of Chemical Engineering, The Pennsylvania State University, University Park, PA, 16802*

‡*Department of Materials Science and Engineering, The Pennsylvania State University, University Park, PA, 16802*

¶*Materials Research Institute, The Pennsylvania State University, University Park, PA, 16802*

E-mail: stm9@psu.edu

Abstract

The Flory Huggins interaction parameter χ quantifies the excess free energy of mixing unlike species, and governs phase behavior in polymer blends and block copolymers. Chain architecture affects how chains pack and interact in the melt, which can significantly influence χ. To explore this, we investigate χ for blends with different architectures of flexible bead-spring chains. We examine blends in which both chain species have a "polypropylene" bead-spring structure, but one species has beads with a slightly weaker interaction: either the side beads (case 1), main chain beads (case 2), or branch point beads (case 3). We use molecular dynamics simulations and thermodynamic integration during "morphing" of one species to another to find χ for all three cases, for which random mixing models would give identical results. We find

the strongest repulsion in the case of side beads, reflecting its higher accessibility to other beads. These systems provide an appealing test for PRISM predictions of structure and miscibility in polymer blends. We supply input to PRISM from simulations without any adjustment, and PRISM predictions are compared directly with simulation results. We find PRISM predictions for χ obtained using the Percus-Yevick (PY) closure (available in public PRISM modules, but problematic in that it incorrectly predicts the dependence of χ on molecular weight) are inconsistent even in their signs and sensitive to the initial guess needed to solve the integral equations.

Introduction

Polymer blends and block copolymers are ubiquitous and have found many applications, as they offer unique and tunable material properties.[1–3] Polymer blends can be miscible or phase-separated or exhibit any degree of mixing between these extremes. Morphology plays an important role in the performance of polymer blends and copolymer mesophases in a given application.[4,5] To tune and optimize the morphology of polymer blends and block copolymers, it is critical to understand their phase behavior, which is governed by the degree of polymerization (N), composition (ϕ), monomer interactions and chain architecture.[2,6]

The Flory-Huggins interaction parameter χ is the excess free energy of mixing different species, arising from monomer interactions and chain architecture. Conceptually, χ measures the free energy cost to place two unlike monomers next to each other. Stronger χ leads to higher free energy costs and a stronger tendency to demix. For demixed systems, further increases in χ result in sharper interfaces between the demixed phases.[2]

χ includes both enthalpic and entropic (packing) effects, which may be written separately as

$$\chi = \chi_S + \frac{\chi_H}{T} \tag{1}$$

For chemically unlike polymers, χ is dominated by enthalpy, as the disparity in cohesive

energy densities makes demixing more likely.[7] For polymers that are chemically similar, differences in chain architecture and monomer geometry (size, shape, chain stiffness, etc.) lead to non-ideal packing in the blend. This contributes entropically to χ, and demixing can still occur for long chains.[8]

Experimentally, it is possible to measure χ, by comparing X-ray or neutron scattering of mixed blends with the Random Phase Approximation (RPA).[9] For highly incompatible mixtures, χ can be obtained by measuring interfacial profiles in bilayers using X-ray or neutron reflectivity.[10]

It is harder to predict χ using simulations. Various methods have been proposed; each has its limitations. One method predicts χ by simulating the interface between segregated phases of a polymer mixture and measuring the interface thickness and composition.[11,12] This method requires the polymer mixture to have $\chi > \chi_{critical}$ and a scheme for rapid equilibration, so that a sharp interface between the segregated phases can be simulated within the simulation volume and equilibrated in a reasonable time. For miscible blends near the critical point, we may calculate χ by measuring composition fluctuations in the simulations and comparing them to RPA. However, to simulate measurable amplitudes in concentration fluctuations, we need reasonably large values for χN, implying the use of long chains in simulations for blends with small values of χ. But if chains are longer than the entanglement length, chains move by reptation, which results in very slow equilibration.

Another method for determining χ involves simulations where a chain is inserted into pure and mixed phases.[13,14] This approach calculates χ from either (a) the ratio of chain insertion probabilities in pure and mixed phases (Widom insertion),[15–17] or (b) the insertion free energy, measured by adding a chain into pure and blend systems, and integrating the thermodynamic work required to insert the chain with respect to the interaction strength.[18–20] But the probability of insertion of a long chain into a melt is low because of the overlap with other chains. Also, since the insertion is made into similar systems, high accuracy for measured values is needed to obtain reliable values for χ.

χ has also been estimated by measuring the cohesive energy densities in simulations of blends.[21–23] Chen et al. used this method with Gibbs ensemble configurational-bias Monte Carlo simulations to determine χ for olefin oligomers.[23] However, because these methods only measure the system energy, they obtain only the energetic contribution to χ.

The Polymer Reference Interaction Site Model (PRISM) has also been used to predict structural and thermodynamic properties associated with polymer miscibility.[24–26] PRISM relates various structural correlation functions between different species in polymer melts and blends. The theory takes the form of coupled non-linear integral equations, which must be solved numerically to obtain the correlation functions, from which χ can be calculated. In its first formulation, PRISM incorrectly predicted the dependence of χ on molecular weight.[27] Later, this shortcoming was remedied with an improved "molecular" closure, which better accounted for the connectivity within molecules.[28]

In our group, we have developed a powerful method for extracting χ of polymer blends from simulations.[8,29] Our approach is related to previous methods for computing solvation free energies, which compute the thermodynamic work to turn on interactions between a solute and the surrounding solvent, and so determine the free energy to transfer a molecule from one phase into another, thereby measuring Henry constants or chemical potential differences between phases.[18] Since our method uses standard molecular dynamics platforms (albeit with manipulations of the interactions, and measurements of nonstandard quantities), it can be used without custom programming of anything other than driver scripts.

In our method, we use molecular dynamics (MD) simulations and a novel thermodynamic integration scheme to compute the thermodynamic work required to transform chains from one species to another. Starting from a reference melt in which all chains are of type 1, we compute the work $\Delta G_{blend} = G_{blend} - G_1$ to transform or "morph" half the chains to type 2, and separately the work $\Delta G_{pure} = G_2 - G_1$ to morph all the chains to type 2. The excess

Gibbs free energy of mixing is

$$\Delta G_{ex} = G^{blend} - \phi_1 G_1 - \phi_2 G_2 = \Delta G_{blend} - \phi_2 \Delta G_{pure} \tag{2}$$

From the excess Gibbs free energy of mixing per bead ΔG_{ex}, we define χ as

$$\beta \Delta G_{ex} = \chi \phi_1 \phi_2 \tag{3}$$

Here, $\beta = 1/k_B T$ (k_B is the Boltzmann constant, T is temperature); ϕ_1 and ϕ_2 are volume fractions of polymer 1 and 2; and G^{blend}, G_1 and G_2 are free energy per bead of the blend, pure component 1, and pure component 2 respectively.

In previous works, we have successfully applied this method to obtain χ as small as 10^{-4} per monomer. Kozuch et al. studied the effect of stiffness mismatch on χ using this method.[8] In the study, bead-spring chains in the blend differed only in their backbone stiffness and experienced repulsive interactions as a result of non-ideal local packing. χ predictions were found to be consistent with experiments for blends of enthalpically similar species, when real polymers were mapped to bead-spring chains. Zhang et al. employed this method to study blends of bead-spring chains with mismatched enthalpic interactions.[29] χ predictions were verified by calculating the interfacial density profile for phase-separated binary mixtures using lattice self-consistent field theory and comparing it with the interfacial density profile from simulations of immiscible blends.

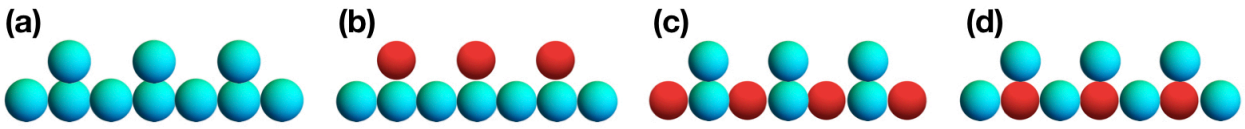

Figure 1: Different types of chains considered in this work: (a) Chain type 1, present in all blends; Chain type 2 for cases of weakly interacting (b) side bead, (c) main bead and (d) branch bead.

Here, we use this method to explore the effect of chain architecture on χ (Figure 1). We

consider binary blends of flexible bead-spring chains, in which both chain species have a structure analogous to polypropylene. Half of the polymer chains in the blend are as shown in (a), while the other half are as either (b), (c) or (d) in Figure 1. The interaction strength of the red beads is weaker than that of the blue beads, with the red-blue interaction given by the usual geometric mean mixing rule appropriate for nonpolar interactions. We have three cases, in which the weakly interacting bead is on the side, main or branch point of the monomer. Random mixing models would predict the same χ for all three blends. However, we intuitively expect chains (b), (c) and (d) will pack and interact differently with chains (a). Hence different chain architecture should result in different phase behavior in the blends. As we shall see below, the strongest repulsive interactions are present in the blend with weakly interacting side beads, which are most accessible to interact with beads on other chains.

We also use our simulations to test PRISM predictions of χ. We obtain single-chain correlation functions between different types of beads in the simulations. We provide these correlations as input to PRISM along with the interaction potential acting between the beads.

We solve PRISM equations numerically using pyPRISM, an open-source python platform for performing PRISM calculations developed by Martin et al.[30] In this way, we obtain PRISM predictions for structural correlations between different beads in the blend and calculate χ from these correlation functions for each case. Spatial correlations between the two types of chains in the blend and correlations between weakly interacting beads are compared with simulation results, to investigate the accuracy of PRISM predictions.

At present, our calculations are limited to use of the local Percus-Yevick closure. The PY "atomic" closure predicts incorrect molecular weight dependence for the critical point χ in symmetric polymer blends, which was eventually remedied by improved "molecular" closures. However, the more complex molecular closures have not yet been implemented in pyPRISM. We find PRISM results for χ are within an order of magnitude of simulation values, albeit sometimes with incorrect signs, and strongly dependent on the initial guess

provided to solve the PRISM equations.

Methods

Morphing simulation details

In our two-component polymer blends, all the bead-spring chains have an architecture analogous to polypropylene. Polymer 1 refers to "reference" chains in which all beads have the same interaction strength. Polymer 2 chains have one weakly interacting bead in each monomer, with the rest of the beads identical to those in polymer 1.

We represent non-bonded interactions between beads with the Lennard-Jones (LJ) potential $U_{LJ}(r)$, given by

$$U_{LJ}(r) = 4\epsilon \left[\left(\frac{\sigma}{r}\right)^{12} - \left(\frac{\sigma}{r}\right)^{6} \right] \tag{4}$$

Here r is the distance between centers of interacting beads, ϵ is the interaction strength, and the LJ potential minimum is located at $\sigma^* = 2^{1/6}\sigma$.

Our idealized flexible bead-spring model is not intended to represent any actual polymer. For example, we use a rather short cutoff $r_c = 2\sigma^*$, as a matter of computational convenience; that is, we define our model polymer to have this interaction potential, rather than introducing it as a poor approximation to the full LJ interaction.

However, to work with familiar "atomistic" magnitudes of length, energy, and time, we choose the bead size σ as 0.2 nm, and the reference interaction strength ϵ as 1 kT (2.49 kJ/mol at 300 K). Likewise, the bead mass m_b is taken as 12 g/mol, so that the Lennard-Jones time τ_{LJ} equals $\sigma(m_b/\epsilon)^{1/2} = 0.44$ ps. The "weakened" beads have a smaller interaction strength, which is controlled by the morphing parameter λ (see below). For interactions between unlike beads, we use geometric average of the interaction parameters.

The bond length between successive beads is taken as σ^*, and bonded interactions are described by a harmonic potential $U_b = \frac{1}{2}k_b(r - \sigma^*)^2$, with spring constant $k_b = 400kT/\sigma^2$.

This spring is quite stiff, and maintains an essentially fixed bond length.

Each chain contains 60 beads (20 monomers), and the system consists of 400 chains. The velocity rescaling thermostat and Berendsen barostat were used to maintain the temperature and pressure. As a consequence of the short cutoff, we use a reasonably large pressure P equal to $0.1kT/\sigma^3$ (517.7 bar) to maintain a melt-like density. All simulations were performed using GROMACS.[31]

First, we obtain an equilibrated melt in which all the chains are of type 1 (reference chains). To build the initial configuration, we stack straight chains in a rectangular array in a simulation box of dimensions $10\times10\times10$ nm. We minimize the system energy, and perform NVT simulation for 100 ps at 300 K to randomize the chain orientations. We then deform the simulation box for 1 ns until the box dimensions reach $6.5\times6.5\times6.5$ nm, corresponding to a nominal melt with bead concentration of 0.7 beads per σ^3. The resized melt is then simulated in an NPT ensemble at $P = 0.1kT/\sigma^3$ and T= 300 K to obtain an equilibrated melt.

To obtain ΔG_{ex}, we perform "morphing" simulations.[8,29] We perform a series of simulations in which the morphing parameter λ increments systematically from 0 to 1, and the interaction strength of the weakened beads is correspondingly reduced linearly from 1 kT to 0.5 kT. The usual geometric mixing rule $\epsilon_{\alpha\beta} = \sqrt{\epsilon_\alpha \epsilon_\beta}$ determines the interaction strength between weakened and reference beads.

If the designated beads in all the chains are weakened, we obtain at $\lambda = 1$ a pure melt of type 2 chains with a weakened bead in every monomer. And if the designated beads in half of the chains are weakened, we obtain at $\lambda = 1$ a blend of type 1 and 2 chains. A typical configuration of the fully morphed blend is shown in Fig. 2.

We then determine the work required to morph the chains by a small increment of λ. The simulations are carried out in NPT ensemble; the Gibbs partition function Z can be

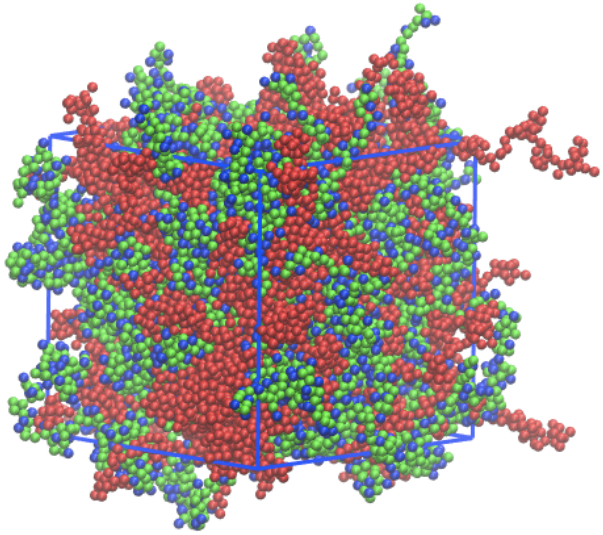

Figure 2: Snapshot of blend with weakly interacting side beads at $\lambda = 1$, i.e., with fully weakened beads. Reference chains without weakened beads are red; chains with weakened beads are green; weakened beads themselves are blue.

written as a sum over microstates r as

$$Z = \sum_r e^{-\beta(E_r(\lambda)+PV_r)} = e^{-\beta G} \tag{5}$$

in which G is the Gibbs free energy. In the partition sum, only the microstate energy $E_r(\lambda)$ depends explicitly on the morphing parameter λ, through its effect on the pair interactions.

Hence we have explicitly

$$\frac{\partial G}{\partial \lambda} = Z^{-1} \sum_r (\partial E_r/\partial\lambda) e^{-\beta(E_r(\lambda)+PV_r)} = \left\langle \frac{\partial E_r}{\partial \lambda} \right\rangle \tag{6}$$

Because only $E_r(\lambda)$ has explicit λ dependence, only $(\partial E_r/\partial\lambda)$ appears in the ensemble average.

Correspondingly, the free energy change on morphing is

$$\Delta G = \int_0^1 d\lambda \left\langle \frac{\partial E_r}{\partial \lambda} \right\rangle \tag{7}$$

That is, ΔG on morphing is the integral with respect to the "displacement" λ of the average "generalized force", which is the corresponding derivative of the energy $\partial E_r/\partial\lambda$. The relationship is precisely analogous to the usual thermodynamic work as the integral of the force, which is the average of $\partial E/\partial x$.

Rather than averaging the actual derivative $\partial E_r/\partial\lambda$, we make a finite difference approximation:

$$\frac{\partial G}{\partial \lambda} \approx \frac{\langle \Delta E_\lambda \rangle}{\Delta \lambda} \tag{8}$$

where ΔE_λ is the change in the system energy for a small change $\Delta\lambda$. To compute this average, we rerun a simulation trajectory at a given λ with interaction parameters corresponding to adjacent λ values. The total energy of the system is measured for the two reruns, and the difference ΔE_λ is divided by $\Delta\lambda$.

Depending on the position of the weakly interacting bead in its monomer, we have three cases (Figure 1): (i) side bead, (ii) main bead, and (iii) branch bead. We have performed simulations and determined χ for all three cases. It is physically clear that the blend with weakened side bead should give the largest χ because the side bead is most accessible to interact with other beads. Likewise, we expect the blend with weakened branch bead to give the smallest χ, as access to this bead is more sterically restricted.

We also perform PRISM calculations for χ and compare with our simulation results for all three cases. Beyond the value of χ itself, we compare two types of spatial correlations obtained from simulations with PRISM predictions: (1) correlation between chain 1 ("reference chains") and chain 2 ("weakened chains"); and (2) correlation between "weakened" beads. These correlations change as we morph the chains. The correlation function between reference and weakened chains exhibits a "correlation hole", as the two chain species begin to avoid each other. The correlation function between weakened beads exhibits a "correlation hill" or increased correlation, as beads begin to clump together. We compare the extent of changes observed in these correlation functions between simulation and PRISM calculations for all three cases.

PRISM theory

PRISM theory describes structural correlations in polymer systems. PRISM requires the input of intra-molecular correlation functions between monomeric species, as well as the interaction potential acting between the species. On solving non-linear integral equations defined in the PRISM theory, we obtain spatial correlations between different species across the system as output. We can calculate χ from the inter-molecular correlation functions describing the polymer blend.[24,30]

In our study, each bead corresponds to an interacting site. For ease of discussion, we introduce notation for different types of beads in the system. We denote all beads in chain type 1 as sites of type A, the beads in chain type 2 with interaction strength identical to A as sites of type B, and weakly interacting beads are sites of type C. The three cases have C beads in three different positions within monomer: the side, main or branch. We could have used a 4-site or even a 6-site convention instead of three site types proposed above, to have a more explicit and symmetric representation of the system. However, with higher number of sites, the matrices of correlation functions in PRISM have higher dimension. We find difficult convergence and numerical inconsistencies when solving PRISM equations for more than three types of sites.

The PRISM integral equation, which relates different spatial correlation functions, is written in Fourier space as

$$\hat{H}(k) = \hat{\Omega}(k) \cdot \hat{C}(k) \cdot [\hat{\Omega}(k) + \hat{H}(k)] \tag{9}$$

Here $\hat{H}(k)$ is the matrix of total correlation functions, $\hat{\Omega}(k)$ is the matrix of intra-molecular correlation functions, and $\hat{C}(k)$ is the matrix of direct correlation functions (conforming to PRISM literature, the caret denotes quantities in Fourier space). For our system with three types of sites, each of these functions is a 3×3 matrix, with different pairwise correlation functions as its elements. PRISM theory has been extensively discussed in literature;[28,30,32–34]

here, for completeness and consistency of notation, we briefly recapitulate the main elements of the theory in Appendix A.

Solving PRISM equations

There are two unknowns in the PRISM equation, $\hat{H}(k)$ and $\hat{C}(k)$; hence an additional "closure relation" is needed. Closure relations relate $H(r)$ and $C(r)$ to the interaction potential $U(r)$. Various closure relations have been proposed, which are approximations based on analogies with atomic fluids.[32] However, PRISM equations implementing these "atomic" closures are known to predict incorrect molecular weight dependence for χ ($1/\sqrt{N}$ instead of $1/N$).[27] The atomic closures ignore chemical bonding mediated indirect interactions between two sites.[32] To remedy this, "molecular" closures have been introduced.[28,32] Unfortunately, molecular closures are not yet available in pyPRISM. In this work, among the available atomic closure relations we use the Percus-Yevick (PY) closure, which in real space is given by

$$c_{\alpha\beta}(r) = \left(1 - e^{\beta U_{\alpha\beta}(r)}\right)\left(h_{\alpha\beta}(r) + 1\right) \tag{10}$$

in which $\beta = 1/k_B T$ (k_B is the Boltzmann constant and T is the temperature). PY has been found to work well for one-component polymer fluids.[32]

With the inputs of intra-molecular correlation functions $\hat{\Omega}(k)$ and the interaction potentials $U_{\alpha\beta}(r)$, we have coupled, non-linear PRISM integral equations and closure relation. To solve these equations numerically within pyPRISM, the PRISM equations are iterated from an initial guess until a consistent solution is found, using a Newton-Krylov numerical method. In the numerical scheme, we use a real-space domain of 8192 grid points with spacing 0.002 nm to represent the various functions, for a total spatial range of greater than 16 nm.

To prepare an initial guess and obtain a solution, we proceed as follows. First, we find the solution to PRISM equations describing a melt of type 1 chains (reference melt), with

sites interacting with the Weeks-Chandler-Anderson (WCA) potential (purely repulsive interactions). This single-component purely repulsive melt is relatively robust to solve with even a zero initial guess. The solution for reference melt with WCA potential is then used as an initial guess to solve the PRISM equations describing the reference melt, with sites interacting with the actual truncated LJ potential (Eqn. 4). In turn, the solution for reference melt with the actual potential is used as an initial guess for solving PRISM equations describing the blend, where half the chains have a weakened bead in every monomer (chain type 2). We thereby obtain the intermolecular total and direct correlation functions $\hat{H}(k)$ and $\hat{C}(k)$.

Using the output of direct correlation functions $\hat{C}(k)$ from PRISM theory, we compute χ using the following equation

$$\chi = \lim_{k\to 0} \frac{\rho}{2}\left[\hat{C}_{AA}(k) + \left(\frac{4}{9}\hat{C}_{BB}(k) + \frac{1}{9}\hat{C}_{CC}(k) + \frac{4}{9}\hat{C}_{BC}(k)\right) - 2\left(\frac{2}{3}\hat{C}_{AB}(k) + \frac{1}{3}\hat{C}_{AC}(k)\right)\right] \tag{11}$$

Here $C_{\alpha\beta}$ are the direct correlation functions between monomers of type α and β, and ρ is the number density of interaction sites. Eqn. 11 is derived in Appendix B.

In this way, we calculate χ for all three cases. We also calculate spatial correlations from intermolecular correlation functions $h_{\alpha\beta}(r)$, including spatial correlations between different chain types (reference and weakened chains) and intermolecular correlation functions between weakened beads. All PRISM calculations were performed using the open-source python module pyPRISM, developed by Martin et al.,[30] which provides a well-documented and user-friendly platform to perform PRISM calculations.

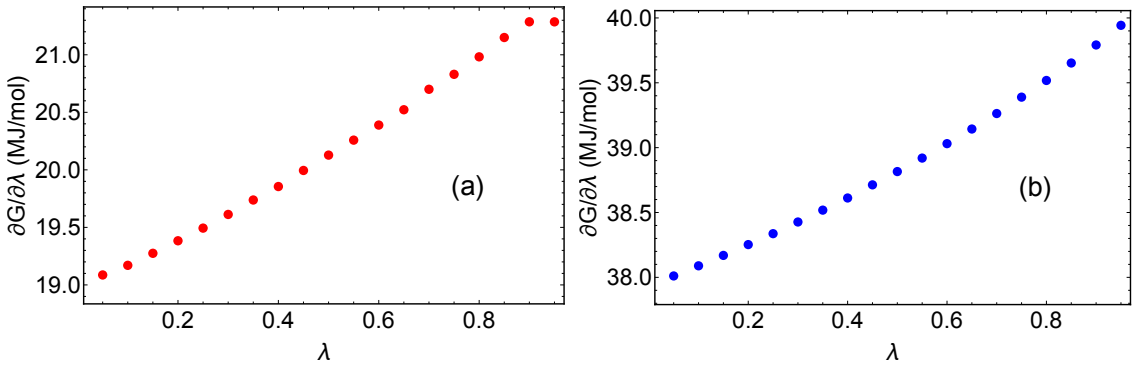

Figure 3: Free energy integrand vs morphing parameter λ for the case of weakly interacting side bead in (a) blend and (b) pure system.

Results and discussion

Simulation

From the morphing simulations for all three cases, we determine the free energy integrand $\partial G/\partial\lambda$ as a function of λ using Eqn. 8, for both blend and pure systems (Figure 3). The excess free energy integrand $\partial G_{ex}/\partial\lambda$ as a function of λ is determined using Eqn. 2 (see Figure 4). Since the area under the curve is positive, there is a free energy cost for mixing such chains, as a result of a mismatch in interaction and packing of chains.

The integrand $\partial G/\partial\lambda$, like any average quantity measured in simulations, has statistical error. To estimate it, we begin by measuring the autocorrelation function of the time series for the numerator ΔE_λ in Eqn. 8, from which we obtain an autocorrelation time τ of about 1 ps. Our simulation trajectories span over 30 ns for each λ value, with data taken every 1ps.

If these measurements are independent, the corresponding statistical error for the integrand, calculated from the the standard deviation of ΔE_λ divided by the square root of the number of measurements, is very small indeed. Error bars for the integrand based on this "short-time" statistical error are much smaller than the points in Figure 3.

However, we expect there are longer relaxation times in the system, corresponding to

concentration fluctuations, leading to weak but long-lived fluctuations in the time series for ΔE_λ. Such fluctuations lead to error in the average integrand that is not so easily estimated, and is presumably the source of the "wandering" of successive integrand points away from the evident linear trend as a function of λ.

Indeed, on general grounds we expect the integrand to at least start out linear in λ, persisting as long as the perturbation from the reference system is reasonably weak. Deviations from the linear trend may thus be regarded as evidence of imperfect averaging, leading to uncertainty in the slope of the integrand, and ultimately to uncertainty in χ. To obtain values for χ and quantify this uncertainty, we fit the integrand $(\partial G_{ex}/\partial\lambda)$ vs λ to a linear function passing through the origin, shown as the dashed lines in Figure 4.

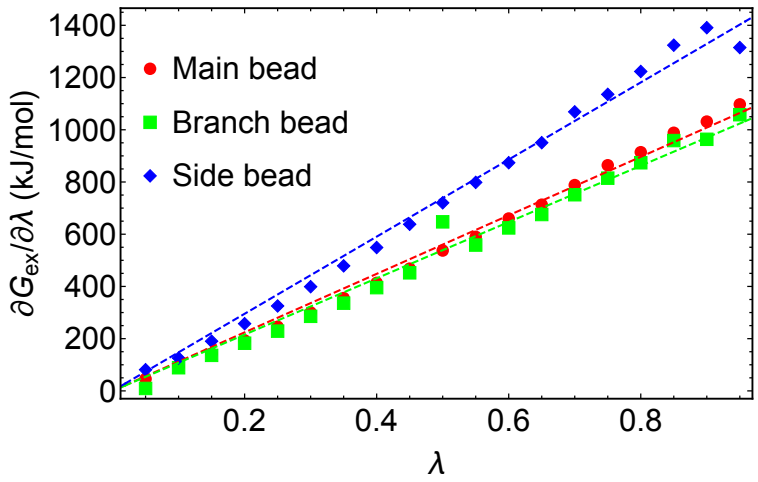

Figure 4: Excess free energy integrand vs morphing parameter λ for the cases of weakened side (blue), main (red) and branch (green) beads. Points are from simulations and the dashed line is a linear fit to the points.

χ is then computed by integrating the fitted linear function for $(\partial G_{ex}/\partial\lambda)$ with respect to λ and dividing the result by the number of beads. The resulting values of χ for all three cases are of the order $O(10^{-2})$ (see Table 1); the corresponding uncertainties for χ reflect the 95 percent confidence intervals for the linear fits. By comparison, error bars computed from the statistical error inferred from a 1 ps correlation time are much smaller, of order $O(10^{-5})$.

The blend with weakly interacting side beads has the largest χ value. χ for blends with weakened main beads or weakened branch beads are essentially equal. Steric accessibility

of the weakly interacting beads explains the order of χ values for the different cases. For weakly interacting side beads, beads from other chains have easier access to the weakened beads.

Table 1: χ from simulations and PRISM theory.

	Simulations			PRISM
Case	χ	χ_V	χ_E	χ
Side	0.0494 ± 0.0012	-0.00184	0.04163	0.0747
Main	0.0375 ± 0.0008	-0.00137	0.0401	0.03385
Branch	0.0361 ± 0.0011	-0.00124	0.039	-0.0105

Like any Gibbs free energy, excess free energy ΔG_{ex} can be written as a sum of three parts:

$$\Delta G = \Delta E - T\Delta S + P\Delta V \tag{12}$$

Correspondingly, the χ value derived from the excess free energy can be regarded as having three contributions,

$$\chi = \chi_E + \chi_S + \chi_V \tag{13}$$

In our simulations, we can measure the change in system energy on morphing, and thereby obtain the energetic contribution to χ. Likewise, the system expands slightly as we morph the designated beads to have weaker interactions, because the weaker attractive interactions lead to a lower density. The volume change contributes to the excess free energy. Table 1 reports the energetic and volume contributions to χ, denoted χ_E and χ_V. Comparing these contributions to the full χ, we see that for these architectures χ is mostly energetic, with only a 10–20% entropic contribution, and a negligible contribution from volume changes. Of course, we would not be able to reach that conclusion without the morphing method to supply the full χ.

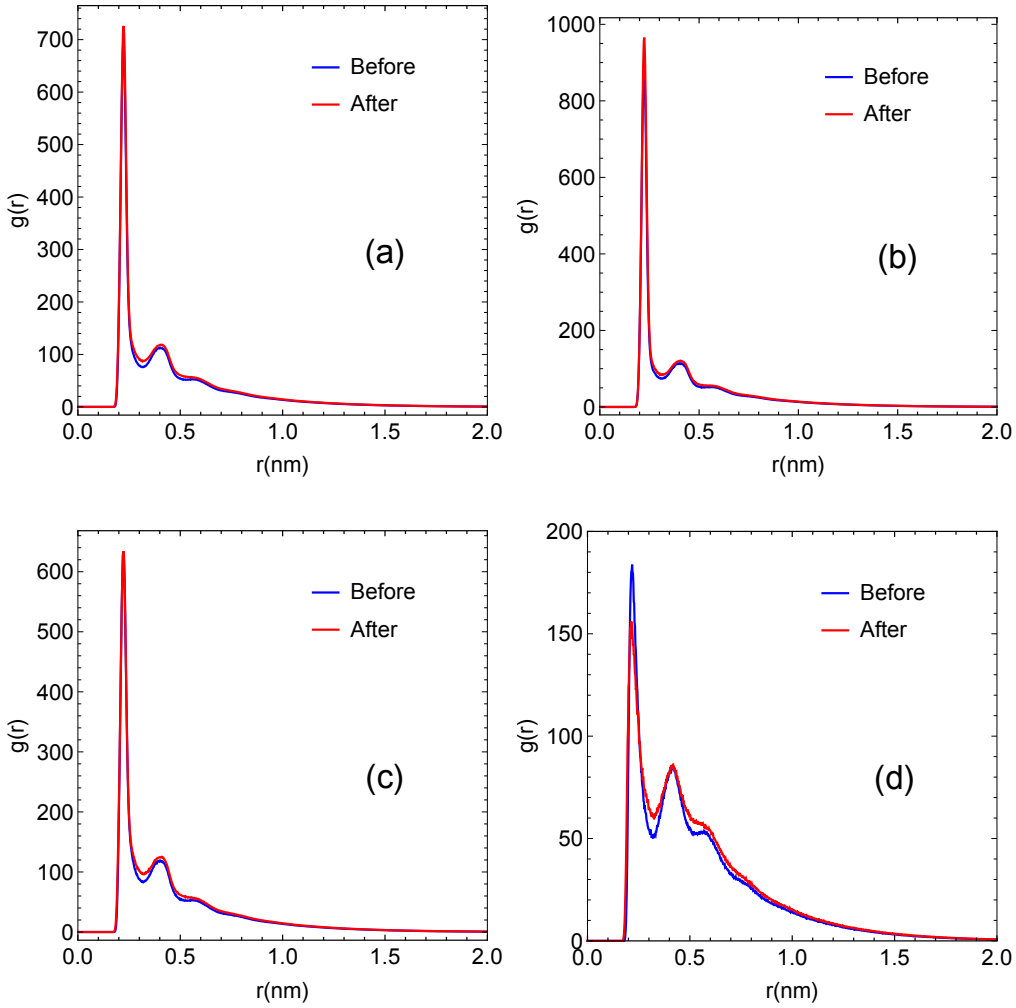

Figure 5: PRISM input for the case of weakened side bead: Intra-chain correlation functions between bead types (a) A-A (b) B-B (c) B-C and (d) C-C, before (blue) and after (red) morphing from the reference melt of identical chains to the pure melt of type 2 chains.

Comparison to PRISM

We test PRISM theory by comparing its predictions for χ with simulation results. We provide as input to PRISM the intra-molecular correlation functions obtained from simulations and the interaction potential between different species. By solving the PRISM equations numerically using the available PY closure, we determine the total and direct intermolecular correlation functions $\hat{H}(k)$ and $\hat{C}(k)$. χ can be determined from $\hat{C}(k)$ using Eqn. 11.

The intra-chain correlations supplied to PRISM were obtained from the simulations of

pure melt of type 2 chains for different cases. The intra-chain correlation functions measured in the melt with weakened side beads are presented in Figure 5 (red curves). Figure 5 also shows the intra-chain correlations obtained from the simulations of reference melts of identical chains (blue curves).

The intra-chain correlation functions obtained from the simulations remain essentially constant as we morph the chains. For weak repulsive interactions per monomer, local configurations are not perturbed significantly. Hence we can supply the intra-chain correlation functions from pure melts as input to PRISM, without worrying whether the correlations were obtained from pure or blend systems. (We have explicitly checked that using the post-morphing intrachain correlation functions as input to PRISM makes essentially no difference in the PRISM predictions.)

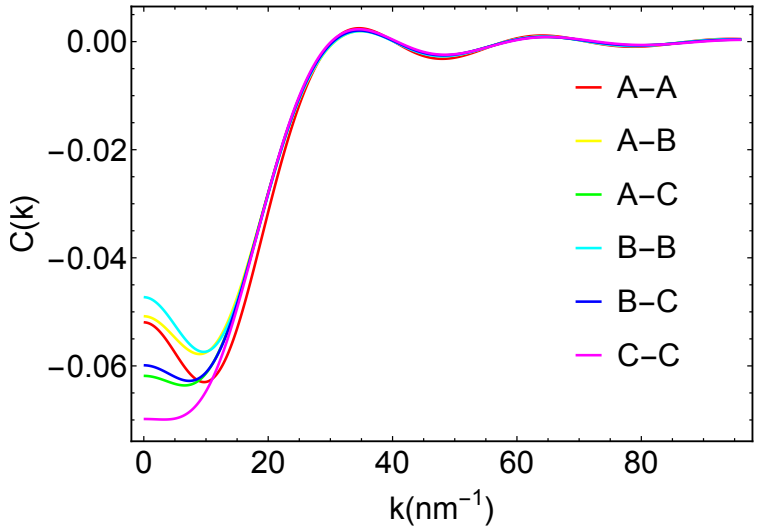

Figure 6: Direct correlation functions $\hat{C}(k)$ for the blend with weakly interacting side beads in half the chains.

Figure 6 shows the PRISM results for $\hat{C}(k)$, for the case of weakly interacting side beads in half the chains in the blend. χ is calculated from $k \to 0$ limit of $\hat{C}(k)$ using Eqn. 11. PRISM predictions for χ for different cases are tabulated in Table.1.

PRISM predictions for χ are only qualitatively consistent with morphing results. PRISM predicts a larger χ than simulation results for weakened side beads, and a negative χ for the

blend with weakened branch beads, for which the morphing result is positive. Only for the case of weakened main beads in the blend does the PRISM χ prediction compare well with simulation results.

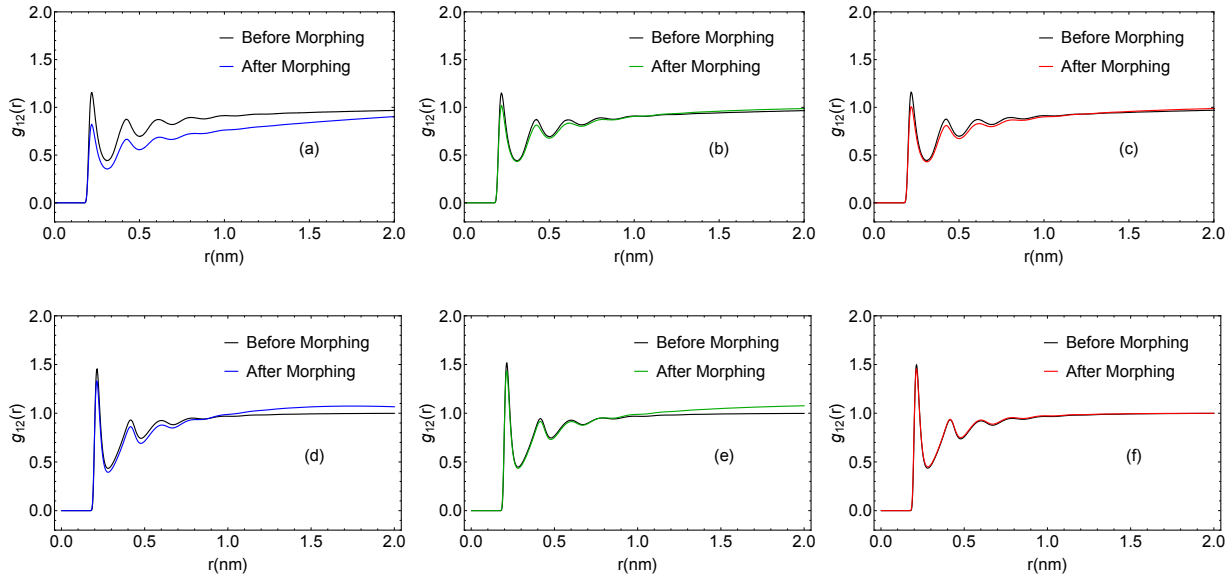

Figure 7: Intermolecular spatial correlation functions between chain type 1 and 2, from simulations (a, b and c) and PRISM (d, e and f) for the cases of side (a,d), main (b,e) and branch (c,f). "Before morphing" = reference melt of identical chains; "After morphing" = final blend.

To investigate the discrepancy in PRISM predictions for χ, we examine its predictions for spatial correlation functions. Firstly, we consider spatial correlations between chains of type 1 (reference) and 2 (weakened) (Figure 7). (The plots focus on the short distance structure for clarity; the correlation functions do all approach unity at large distances.) Local repulsive interactions lead to a dampened correlation between the two types of chains at intermediate distances (Figure 7 (a)-(c)). This effect is strongest for the blend with weakened side beads in type 2 chains, owing to easier access for the other beads to interact with weakened beads. For the cases of weakened main or branch beads in the blend, there is only a very small reduction in correlations between the two types of chains.

Correlation functions obtained from PRISM differ from the simulation results, with regard to the appearance of correlation holes between reference and weakened chains. Com-

paring Figure 7 (a) and (d), for weakened side beads, PRISM predicts a smaller reduction in correlations at intermediate distances after morphing. But PRISM predicts a higher χ compared to simulations for the blend containing chains with weakened side beads (Table 1). Likewise, comparing (b) and (c) with (e) and (f) respectively in Figure 7, PRISM predicts almost no change in correlations at intermediate distances for the cases of weakened main and branch beads. But PRISM χ is positive for the blend with weakened main beads in type 2 chains and negative for the blend containing weakened branch beads in half the chains.

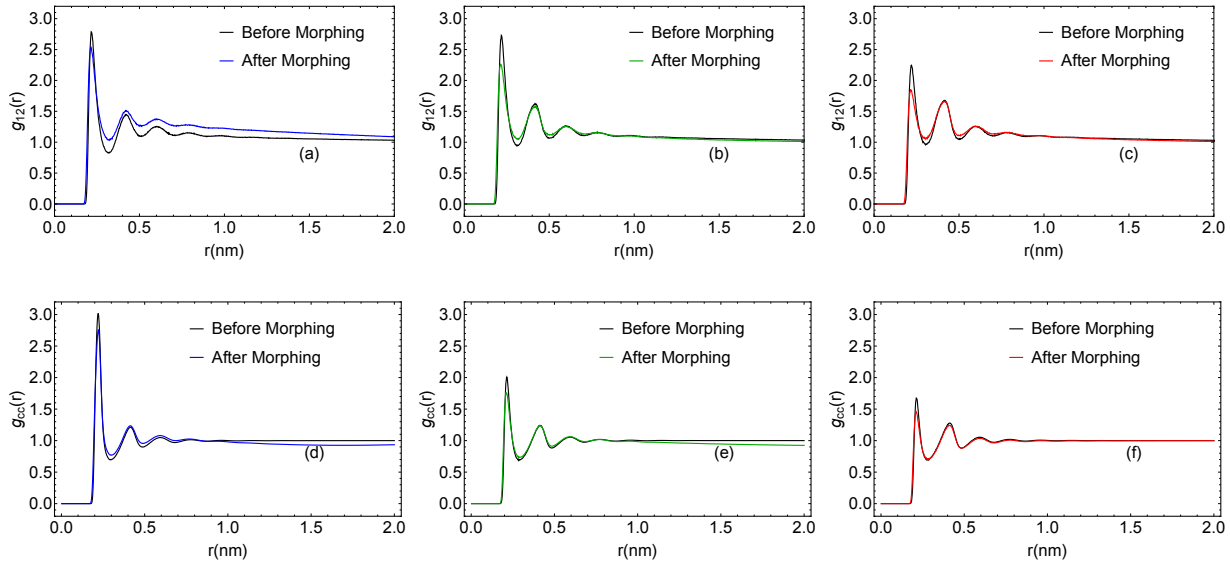

Figure 8: Intermolecular spatial correlation functions between weakly interacting beads (Bead type C), from simulations (a, b and c) and PRISM (d, e and f) for the cases of side (a,d), main (b,e) and branch (c,f). "Before morphing" = reference melt of identical chains; "After morphing" = final blend.

Figure 8 compares simulation results and PRISM predictions for intermolecular correlations between weakened beads in the blend. After morphing, there will be a heightened correlation between weakened beads, as beads with like interactions tend to clump together. The correlation should be strong in the blend containing weakened side beads, and weak for the cases of weakened main beads and branch beads, because of the differences in steric accessibility. This behavior is found for correlations from simulations (Figure 8 (a)-(c)), but not in PRISM predictions.

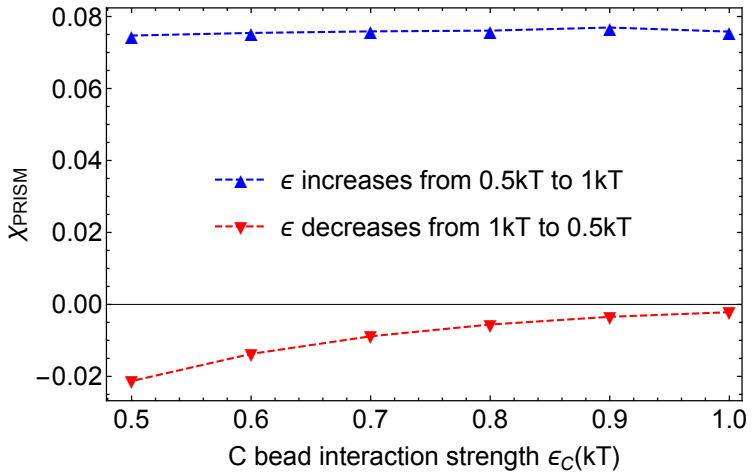

Figure 9: Initial guess dependent χ vs strength of weakly interacting bead ϵ_C: ϵ_C for initial guess incremented from 0.5 kT to 1 kT (blue) and decremented from 1 kT to 0.5 kT (red).

Disturbingly, our PRISM predictions for χ depend qualitatively on the details of the initial guess used to solve the integral equations. For the results reported so far, the procedure for providing an initial guess for the solution to PRISM equations was as described in Section "Solving PRISM equations". However, if we use a different initial guess scheme, we obtain a different value for χ.

For example, for the blend with weakened side beads, we employed a different initial guess scheme. First, we obtain the solution for a system in which all beads have interaction described by LJ potential and strength $\epsilon = 1$ kT, using the solution of reference melt and WCA potential as the initial guess. We then systematically reduced ϵ_C from 1 kT to 0.5 kT, using the solution from the previous step as the initial guess in the given step. As shown in Figure 9 (red points), the resulting χ values are all negative. In a different scheme, we systematically increased ϵ_C from 0.5 kT to 1 kT. The first solution for $\epsilon_C = 0.5kT$ is obtained by using the solution with $\epsilon_C = 1kT$ as the initial guess, and subsequent initial guesses obtained from the previous solution. Then we obtain positive χ values through all the steps (blue curve). Even when ϵ_C reaches 1 kT, χ does not reduce to zero. It is difficult to ascertain which χ is to be believed.

The discrepancies in PRISM predictions may be in part an artifact of our use of atomic

PY closure in PRISM calculations. Atomic closures are known to give incorrect dependence of χ on molecular weight in earlier PRISM studies.[28,32,35] They fail to accurately capture the effect of connectivity on spatial correlations between different species.[32] Molecular closures have been formulated, which take a more explicit account of bond mediated correlations. However, pyPRISM does not at present implement molecular closures; we look forward to an enhanced version of this useful platform, with which a test of χ predictions from molecular closures may be performed.

Conclusions

In this work, we employ molecular dynamics simulations and a novel thermodynamic integration scheme to study how chain architecture affects χ. We "morph" the system from a one-component melt to two-component blend in a series of simulations in which the interaction strength of designated beads is systematically weakened. We integrate the work required to morph over the varying interaction strength, to determine the excess free energy. Our method combines the power of MD simulations to efficiently sample and average thermodynamic quantities, with thermodynamic integration over a well-defined path to obtain values for χ.

Depending on the position of weakened bead in the monomer, we obtain χ for different architectures. The blend containing chains with weakened interactions on the side bead gives the strongest χ. This is physically reasonable, because it is easier for beads on other chains to approach a side bead, compared to a main or branch bead.

Our simulations also present a good test case for PRISM calculations. We can provide single-chain correlations from simulations as input and solve the PRISM equations. Because the simulations directly supply the necessary intrachain correlation functions, no approximate or model intrachain correlation functions need be used when comparing PRISM predictions with simulation results.

Our PRISM predictions for χ are only qualitatively consistent with morphing results. For the blend with weakened side beads in half the chains, χ predicted from PRISM is higher than the value from simulations (and depends on the initial guess). For weakened main beads, PRISM and simulations predict similar values. For weakened branch beads, PRISM gets the sign wrong for χ. PRISM calculations also exhbit sensitivity to the initial guess required to solve the theory numerically. Depending on the scheme adopted for initial guesses, we can obtain completely different χ values.

The discrepancies in PRISM predictions may in part result from our use of atomic closures. We have used pyPRISM, an open-source python module which at present only implements local atomic closures. It has been shown that atomic closures do not properly account for the effects of molecular connectivity on structural correlations. When molecular closures are implemented in pyPRISM, we will revisit the predictions for these bead-spring models.

Appendix A: Elements of PRISM theory

The total correlation function $\hat{H}(k)$ describes the correlation between the position of different sites in the blend. (Here and throughout, the caret $\hat{}$ denotes quantities in Fourier space.) Our system has three different kinds of sites, denoted A, B, and C:

$$\hat{H}(k) = \begin{bmatrix} \rho_{AA}^{pair}\hat{h}_{AA}(k) & \rho_{AB}^{pair}\hat{h}_{AB}(k) & \rho_{AC}^{pair}\hat{h}_{AC}(k) \\ \rho_{BA}^{pair}\hat{h}_{BA}(k) & \rho_{BB}^{pair}\hat{h}_{BB}(k) & \rho_{BC}^{pair}\hat{h}_{BC}(k) \\ \rho_{CA}^{pair}\hat{h}_{CA}(k) & \rho_{CB}^{pair}\hat{h}_{CB}(k) & \rho_{CC}^{pair}\hat{h}_{CC}(k) \end{bmatrix} \tag{14}$$

Here $\rho_{\alpha\beta}^{pair} = \rho_\alpha \rho_\beta$, where ρ_α and ρ_β are the number density of site types α and β. The real-space function $h_{\alpha\beta}(r)$ is given by $h_{\alpha\beta}(r) = g_{\alpha\beta}(r) - 1$, where $g_{\alpha\beta}(r)$ is the intermolecular pair correlation function.

One necessary input for PRISM is the matrix of intra-molecular correlation functions $\hat{\Omega}(k)$. Information about the chain chemical structure and connectivity is encoded in $\Omega(r)$.

$\hat{\Omega}(k)$ for a three-component system is given by

$$\hat{\Omega}(k) = \begin{bmatrix} \rho_{AA}^{site}\hat{\omega}_{AA}(k) & \rho_{AB}^{site}\hat{\omega}_{AB}(k) & \rho_{AC}^{site}\hat{\omega}_{AC}(k) \\ \rho_{BA}^{site}\hat{\omega}_{BA}(k) & \rho_{BB}^{site}\hat{\omega}_{BB}(k) & \rho_{BC}^{site}\hat{\omega}_{BC}(k) \\ \rho_{CA}^{site}\hat{\omega}_{CA}(k) & \rho_{CB}^{site}\hat{\omega}_{CB}(k) & \rho_{CC}^{site}\hat{\omega}_{CC}(k) \end{bmatrix} \tag{15}$$

where $\rho_{\alpha\beta}^{site} = (\rho_\alpha + \rho_\beta)$ if $\alpha \neq \beta$, else $\rho_{\alpha\beta}^{site} = \rho_\alpha$.

$\hat{\omega}_{\alpha\beta}(k)$ are intrachain correlation functions, between species α and β present within a chain. This means that $\hat{\Omega}(k)$ is "block diagonal", with each block corresponding to the species present on a given type of chain. For our system, the reference chain has only sites of type A, while the weakened chain has sites of type B and C.

$\hat{\omega}(k)$ is often supplied using analytical expressions, that approximately represent various chemical structures and architectures. Here, we use simulations to provide these correlations without any approximation. We obtain $\hat{\omega}_{\alpha\beta}(k)$ from simulations by measuring the intra-chain pair distribution function $g_{\alpha\beta}^{intra}(r)$, which is related to $\hat{\omega}_{\alpha\beta}(k)$ via

$$\hat{\omega}_{\alpha\beta}(k) = \begin{cases} \rho \int g_{\alpha\beta}^{intra}(r) \frac{\sin(kr)}{kr}\ r^2 dr, & \text{if } \alpha \neq \beta \\ 1 + \rho \int g_{\alpha\beta}^{intra}(r) \frac{\sin(kr)}{kr}\ r^2 dr, & \text{if } \alpha = \beta \end{cases} \tag{16}$$

This relation was derived from Debye scattering equation[30,36]

$$\hat{\omega}_{\alpha\beta}(k) = \left\langle \frac{1}{N^{total}} \sum_{i}^{N_\alpha} \sum_{j}^{N_\beta} \frac{\sin(kr_{ij})}{kr_{ij}} \right\rangle \tag{17}$$

in which $N^{total} = N_\alpha + N_\beta$ when $\alpha \neq \beta$, else $N^{total} = N_\alpha$. Here N_α is the number of sites of type α present within a given chain.

As stated above, for our system $\hat{\omega}_{AB}(k) = \hat{\omega}_{AC}(k) = 0$, as beads A do not reside in the same chains as B and C. We obtain $g_{\alpha\beta}^{intra}(r)$ from simulations of pure melt of type 2 chains, the system obtained after morphing all the chains in the system. These correlation

functions are nearly identical to those from those obtained from the blend, as the local structures are not affected significantly by small changes in surrounding conditions (see Fig. 5). The second input needed to solve the PRISM equation are the interaction potentials $U_{\alpha\beta}(r)$ acting between different types of sites.

The direct correlation function $\hat{C}(k)$ is obtained by solving the PRISM equation. $\hat{C}(k)$ is written as

$$\hat{C}(k) = \begin{bmatrix} \hat{c}_{AA}(k) & \hat{c}_{AB}(k) & \hat{c}_{AC}(k) \\ \hat{c}_{BA}(k) & \hat{c}_{BB}(k) & \hat{c}_{BC}(k) \\ \hat{c}_{CA}(k) & \hat{c}_{CB}(k) & \hat{c}_{CC}(k) \end{bmatrix} \tag{18}$$

Here $\hat{c}_{\alpha\beta}$(k) is the direct intermolecular site-site correlation function between sites of type α and β. The matrix of structure factors $\hat{S}(k)$ is related to $\hat{H}(k)$ and $\hat{\Omega}(k)$ through

$$\hat{S}(k) = \hat{\Omega}(k) + \hat{H}(k) \tag{19}$$

Substituting Eqn. 19 into Eqn. 9 we have

$$\hat{S} = \hat{\Omega} + \hat{\Omega} \cdot \hat{C} \cdot \hat{\Omega} + \hat{\Omega} \cdot \hat{C} \cdot \hat{\Omega} \cdot \hat{C}\hat{\Omega} + \ldots \tag{20}$$

Hence beads at two different sites are correlated through $\hat{\Omega}(k)$ as they are on the same chain, or they are on different chains and interact via $\hat{C}(k)$, and so forth. Therefore $\hat{C}(k)$ represents the effective potential acting between the sites.

Appendix B: χ from direct correlation function $\hat{C}(k)$

The free energy (or effective Hamiltonian) of concentration fluctuations is given by

$$\beta\partial G = \frac{1}{2} \sum_{\alpha,\beta} \int d^3k \; \hat{\psi}^*_\alpha(k) \hat{S}^{-1}_{\alpha\beta}(k) \hat{\psi}_\beta(k) \tag{21}$$

Here $\hat{\psi}_\alpha$ is fluctuation in the concentration of site type α. $\hat{S}^{-1}_{\alpha\beta}$ are the elements of the matrix inverse of $\hat{S}$.

Using equations 19 and 9, the inverse structure factor matrix $\hat{S}^{-1}(k)$ can be written as

$$\hat{S}^{-1} = \hat{\Omega}^{-1} - \hat{C} \tag{22}$$

We are interested in χ in the $k \to 0$ limit. In this limit, the intra-chain correlation function $\hat{\omega}_{\alpha\beta}(k)$ (Eqn. 17) simplifies, and the matrix elements $\hat{\Omega}(k)_{\alpha\beta}$ reduce to

$$\begin{aligned}
\hat{\Omega}(k \to 0)_{\alpha\beta} &= \frac{N_\alpha N_\beta}{N_T} \rho^{site}_{\alpha\beta} \\
&= \frac{N_\alpha N_\beta}{V} n_i \\
&= \frac{N_\alpha N_\beta}{n_i} \phi_i \rho \\
&= f^{(i)}_\alpha f^{(i)}_\beta n_i \phi_i \rho
\end{aligned} \tag{23}$$

Here i denotes the type of chain corresponding to the block of the matrix $\hat{\Omega}$ we are considering; n_i is the number of chains of type i, ϕ_i their volume fraction, N_i the number of sites per chain, and $f^{(i)}_\alpha$ the fraction of sites of type α on chains of type i. Finally, V is the volume of the system, and ρ the total number density of sites in the system. Here we assume that the volume of all sites is equal.

Evidently, each block in the matrix $\hat{\Omega}$ is a scalar $n_i \phi_i \rho$, times a dyad of vectors of site fractions $f^{(i)}_\alpha$. That is, each block of the matrix is proportional to a projection operator, which projects any vector of concentration fractions onto the site fractions present on chains of type i.

Projection operator matrices of the form $F_\alpha F_\beta$ cannot be fully inverted; they have a nullspace, consisting of all vectors orthogonal to F. Hence $\hat{\Omega}$ as well as $\hat{S}$, which can be written as a series expansion (Eqn. 19), cannot be fully inverted. This singularity is a consequence of the fact that at long wavelengths, a fluctuation must satisfy the condition

that the different sites appear at specified fractions on a given type of chain.

So we invert the matrix $\hat{\Omega}$ in the subspace of fluctuations proportional to vectors $f_\alpha^{(i)}$ for each chain type. The limited inverse satisfies the condition $\hat{\Omega} \cdot \hat{\Omega}^{-1} \cdot \hat{\Omega} = \hat{\Omega}$, which can be solved as

$$\hat{\Omega}^{-1}_{\alpha\beta} = \frac{f_\alpha^{(i)} f_\beta^{(i)}}{n_i \phi_i \rho (f^{(i)} \cdot f^{(i)})^2} \tag{24}$$

where $f^{(i)} \cdot f^{(i)}$ is the square of the site fraction vector $f_\alpha^{(i)}$ for chain type i.

The monomer concentrations within each chain type i must be proportional to $f_\alpha^{(i)}$, so at long wavelengths, we can write the concentration fluctuations as

$$\hat{\psi}_\alpha(k \to 0) = \sum_i f_\alpha^{(i)} \delta\phi_i \tag{25}$$

Furthermore, since the system is incompressible, the sum of concentration fluctuations $\sum_i \delta\phi_i$ must vanish everywhere. If we have two kinds of chain, we must have $\delta\phi_1 = -\delta\phi_2$. So the entire set of concentration fluctuations of all the species α can be thus be written as proportional to $\delta\phi_1$.

Using Eqn. 22, Eqn. 24, and with $\delta\phi_2 = -\delta\phi_1$ we simplify the free energy of concentration fluctuations at long wavelengths to

$$\beta\partial G = \frac{1}{2}\delta\phi_1^2 \left(\frac{1}{N_1\phi_1\rho} + \frac{1}{N_2\phi_2\rho} - \left(\sum_{\alpha\beta} f_\alpha^{(1)} f_\beta^{(1)} c_{1\alpha,1\beta} + \sum_{\alpha\beta} f_\alpha^{(2)} f_\beta^{(2)} c_{2\alpha,2\beta} - 2\sum_{\alpha\beta} f_\alpha^{(1)} f_\beta^{(2)} c_{1\alpha,2\beta} \right) \right) \tag{26}$$

Here $c_{i\alpha,j\beta}$ denotes the direct correlation function between sites of type α on chains of type i and sites of type β on chains of type j, (recall $f_\alpha^{(i)}$ is the fraction of sites of type α on chains of type i). Effectively, Eqn. 26 expresses the direct correlation c_{ij} between chains of type i and type j, with a weighted average over the different kinds of monomers on each chain.

Comparing this form to the usual RPA expression, we identify χ as

$$\chi = \frac{\rho}{2}\left(\bar{c}_{11} + \bar{c}_{22} - 2\bar{c}_{12}\right) \tag{27}$$

Here we have defined the weighted average $\bar{c}_{ij}$ as

$$\bar{c}_{ij} = \sum_{\alpha\beta} f_{\alpha}^{(i)} f_{\beta}^{(j)} c_{i\alpha,j\beta} \tag{28}$$

in which all direct correlation functions are understood to be evaluated in the limit $k \to 0$.

For the particular case of interest in this work, chains of type 1 have only monomers of type A, while chains of type 2 have sites of type B and C, with $f_B^{(2)} = 2/3$ and $f_C^{(2)} = 1/3$. Hence we have

$$\begin{aligned}
\bar{c}_{11} &= c_{1A,1A} \\
\bar{c}_{22} &= (4/9)c_{2B,2B} + (4/9)c_{2B,2C} + (1/9)c_{2C,2C} \\
\bar{c}_{12} &= (2/3)c_{1A,2B} + (1/3)c_{1A,2C}
\end{aligned} \tag{29}$$

Finally, since monomers of type A only occur on chains of type 1, and monomers of types B and C only occur on chains of type 2, we can silently drop the 1 and 2 subscripts on the right side of the above equations.

Acknowledgement

We would like to thank Dr. Arthi Jayaraman, Dr. Tyler B. Martin, and Dr. Thomas E. Gartner III for helpful discussion about PRISM and pyPRISM. Financial support from the National Science Foundation under awards DMREF-1629006 and DMREF-1921854 are acknowledged.

References

(1) Shaw, M. T. Processing and commercial application of polymer blends. *Polymer Engineering & Science* **1982**, *22*, 115–123.

(2) Bates, C. M.; Bates, F. S. 50th Anniversary Perspective: Block Polymers—Pure Potential. *Macromolecules* **2017**, *50*, 3–22.

(3) Robeson, L. M. Applications of polymer blends: Emphasis on recent advances. *Polymer Engineering & Science* **1984**, *24*, 587–597.

(4) Tao, Y.; McCulloch, B.; Kim, S.; Segalman, R. A. The relationship between morphology and performance of donor–acceptor rod–coil block copolymer solar cells. *Soft Matter* **2009**, *5*, 4219–4230.

(5) Guo, C.; Lin, Y.-H.; Witman, M. D.; Smith, K. A.; Wang, C.; Hexemer, A.; Strzalka, J.; Gomez, E. D.; Verduzco, R. Conjugated Block Copolymer Photovoltaics with near 3% Efficiency through Microphase Separation. *Nano Letters* **2013**, *13*, 2957–2963, PMID: 23687903.

(6) Rubinstein, M.; Colby, R. *Polymer Physics*; Oxford: Oxford University Press, 2003.

(7) Bates, F. S.; Fredrickson, G. H. Block Copolymer Thermodynamics: Theory and Experiment. *Annual Review of Physical Chemistry* **1990**, *41*, 525–557, PMID: 20462355.

(8) Kozuch, D.; Zhang, W.; Milner, S. Predicting the Flory-Huggins χ Parameter for Polymers with Stiffness Mismatch from Molecular Dynamics Simulations. *Polymers* **2016**, *8*, 241.

(9) Leibler, L. Theory of Microphase Separation in Block Copolymers. *Macromolecules* **1980**, *13*, 1602–1617.

(10) Russell, T. X-ray and neutron reflectivity for the investigation of polymers. *Materials Science Reports* **1990**, *5*, 171 – 271.

(11) Groot, R. D.; Warren, P. B. Dissipative particle dynamics: Bridging the gap between atomistic and mesoscopic simulation. *The Journal of Chemical Physics* **1997**, *107*, 4423–4435.

(12) Chremos, A.; Nikoubashman, A.; Panagiotopoulos, A. Z. Flory-Huggins parameter χ, from binary mixtures of Lennard-Jones particles to block copolymer melts. *The Journal of Chemical Physics* **2014**, *140*, 054909.

(13) Kumar, S. K.; Szleifer, I.; Panagiotopoulos, A. Z. Determination of the chemical potentials of polymeric systems from Monte Carlo simulations. *Phys. Rev. Lett.* **1991**, *66*, 2935–2938.

(14) Villa, A.; Mark, A. E. Calculation of the free energy of solvation for neutral analogs of amino acid side chains. *Journal of Computational Chemistry* **2002**, *23*, 548–553.

(15) Widom, B. Some Topics in the Theory of Fluids. *The Journal of Chemical Physics* **1963**, *39*, 2808–2812.

(16) Dickman, R.; Hall, C. K. Equation of state for athermal lattice chains. *The Journal of Chemical Physics* **1986**, *85*, 3023–3026.

(17) Olsen, R.; Kvamme, B.; Kuznetsova, T. Free energy of solvation and Henry's law solubility constants for mono-, di- and tri-ethylene glycol in water and methane. *Fluid Phase Equilibria* **2016**, *418*, 152 – 159, Special Issue covering the Nineteenth Symposium on Thermophysical Properties.

(18) de Pablo, J. J.; Laso, M.; Suter, U. W. Estimation of the chemical potential of chain molecules by simulation. *The Journal of Chemical Physics* **1992**, *96*, 6157–6162.

(19) Escobedo, F. A.; de Pablo, J. J. Expanded grand canonical and Gibbs ensemble Monte Carlo simulation of polymers. *The Journal of Chemical Physics* **1996**, *105*, 4391–4394.

(20) Stubbs, J. M.; Siepmann, J. I. Aggregation in Dilute Solutions of 1-Hexanol in n-Hexane: A Monte Carlo Simulation Study. *The Journal of Physical Chemistry B* **2002**, *106*, 3968–3978.

(21) Maranas, J. K.; Mondello, M.; Grest, G. S.; Kumar, S. K.; Debenedetti, P. G.; Graessley, W. W. Liquid Structure, Thermodynamics, and Mixing Behavior of Saturated Hydrocarbon Polymers. 1. Cohesive Energy Density and Internal Pressure. *Macromolecules* **1998**, *31*, 6991–6997.

(22) Maranas, J. K.; Kumar, S. K.; Debenedetti, P. G.; Graessley, W. W.; Mondello, M.; Grest, G. S. Liquid Structure, Thermodynamics, and Mixing Behavior of Saturated Hydrocarbon Polymers. 2. Pair Distribution Functions and the Regularity of Mixing. *Macromolecules* **1998**, *31*, 6998–7002.

(23) Chen, Q. P.; Chu, J. D.; DeJaco, R. F.; Lodge, T. P.; Siepmann, J. I. Molecular Simulation of Olefin Oligomer Blend Phase Behavior. *Macromolecules* **2016**, *49*, 3975–3985.

(24) Schweizer, K. S.; Curro, J. G. Integral equation theory of the structure and thermodynamics of polymer blends. *The Journal of Chemical Physics* **1989**, *91*, 5059–5081.

(25) Yethiraj, A.; Kumar, S.; Hariharan, A.; Schweizer, K. S. Surface segregation in polymer blends due to stiffness disparity. *The Journal of Chemical Physics* **1994**, *100*, 4691–4694.

(26) Li, H.; Curro, J. G.; Wu, D. T.; Habenschuss, A. X-ray Scattering of Vinyl Polyolefin Liquids and Random Copolymers: Theory and Experiment. *Macromolecules* **2008**, *41*, 2694–2700.

(27) Deutsch, H. P.; Binder, K. Evidence Against the Integral Equation Theory of Polymer Blends. *Europhysics Letters (EPL)* **1992**, *17*, 697–702.

(28) Yethiraj, A.; Schweizer, K. S. Integral equation theory of polymer blends: Numerical investigation of molecular closure approximations. *The Journal of Chemical Physics* **1993**, *98*, 9080–9093.

(29) Zhang, W.; Gomez, E. D.; Milner, S. T. Predicting Flory-Huggins χ from Simulations. *Phys. Rev. Lett.* **2017**, *119*, 017801.

(30) Martin, T. B.; Gartner, T. E.; Jones, R. L.; Snyder, C. R.; Jayaraman, A. pyPRISM: A Computational Tool for Liquid-State Theory Calculations of Macromolecular Materials. *Macromolecules* **2018**, *51*, 2906–2922.

(31) Van Der Spoel, D.; Lindahl, E.; Hess, B.; Groenhof, G.; Mark, A. E.; Berendsen, H. J. C. GROMACS: Fast, flexible, and free. *Journal of Computational Chemistry* **2005**, *26*, 1701–1718.

(32) Schweizer, K. S.; Yethiraj, A. Polymer reference interaction site model theory: New molecular closures for phase separating fluids and alloys. *The Journal of Chemical Physics* **1993**, *98*, 9053–9079.

(33) Heine, D. R.; Grest, G. S.; Curro, J. G. In *Advanced Computer Simulation: Approaches for Soft Matter Sciences I*; Dr. Holm, C., Prof. Dr. Kremer, K., Eds.; Springer Berlin Heidelberg: Berlin, Heidelberg, 2005; pp 209–252.

(34) Schweizer, K. S.; Honnell, K. G.; Curro, J. G. *The Journal of Chemical Physics* **1992**, *96*, 3211–3225.

(35) Yethiraj, A.; Schweizer, K. S. On the scaling of the critical temperature with the degree of polymerization in symmetric polymer blends. *The Journal of Chemical Physics* **1992**, *97*, 5927–5930.

(36) McCoy, J. D.; Honnell, K. G.; Curro, J. G.; Schweizer, K. S.; Honeycutt, J. D. Single-chain structure in model polyethylene melts. *Macromolecules* **1992**, *25*, 4905–4910.

Graphical TOC Entry